12WCEE 2000

THE SOURCE INVERSION WITH ELEMENT SOURCE WAVEFORMS INCLUDING RUPTURE DIRECTIVITY ON EACH SUBFAULT BY CONVOLUTION TECHNIQUE

Haruko SEKIGUCHI[1], Kojiro IRIKURA[2] And Tomotaka IWATA[3]

SUMMARY

In order to get knowledge about the physics of earthquake rupturing more precisely and to obtain reliable source process for near-source ground motion simulation, we introduced a convolution method (Ben-Menahem, 1961) which incorporate the effect of moving dislocation over a rectangular area to a point source synthetic into computation of element source waves for the waveform inversion. Therefore, the rupture directivity effect on the entire fault area is fully considered in the waveform inversion. The rupture process inverted using this technique has a smooth slip distribution even inside the subfaults. Obtained moment release history on each subfault directly reflects a slip time function on the subfault because the rupture propagation effect inside each subfault is separated. Validity of this technique is based on the following approximation; the Green's functions from two point sources are approximately the same after phase correction when the distances between two point sources is much smaller than the distance between the sources and an observation station. The condition to validate the usage of this technique has been found through numerical tests in our previous work. We applied this technique in the waveform inversion for the source process of the 1995 Hyogo-ken Nanbu earthquake. The global characteristics of moment release distributions are similar between two inversion results; one inverted with point source element waveforms and the other with element source waves considering the finite moving dislocation effects inside each subfault. But details like places of peak moment releases differ between these inversion results. Positive correlation between final slip and peak slip velocity are observed.

INTRODUCTION

Usually, a source fault in the waveform inversion used to be represented by a set of point sources placed at several kilometers intervals on planar surfaces. Such techniques have the following problems.

(1) Each point source is assumed to represent a sum of moment release around it, but a wave from each of the point sources does not include rupture directivity effect itself. In this case, the rupture directivity from the total source is realized by overlapping of waves from an aggregate of the point sources. Therefore the amplitudes of the waves from the entire source area in forward directivity region are underestimated. And on the contrary, those in the backward directivity region are overestimated (Fig.1, left). The rupture directivity effect is caused by coherent overlappings of waves. It is expected that coherent overlapping of waves be gradually suppressed as the frequency of the waves become higher because of heterogeneity of wave-propagation and rupture process. Somerville et al. (1997) showed this phenomenon in observations in near-source area. They showed that the rupture directivity effect is remarkable in period longer than 0.6s. The frequency range of our waveform inversion is 0.1 to 1.0 Hz where the directivity effect might be strongest according to Somerville et al. (1997). Using element waves with no rupture propagation inside the subfaults in the waveform inversion, misestimation of the moment release values may happen depending on the distribution of observation stations. (2) Obtained

[1] *Disaster Prevention Research Institute, Kyoto University, Kyoto, Japan E-mail: haru@egmdpri01.dpri.kyoto-u.ac.jp*
[2] *Disaster Prevention Research Institute, Kyoto University, Kyoto, Japan*
[3] *Disaster Prevention Research Institute, Kyoto University, Kyoto, Japan*

moment release history on each point source includes both slip time function and rupture propagation effect inside each subfault. It is impossible to separate them because rupture propagation inside each subfault is not defined.
(3) Recently, total wave field modeling considering both of source process and wave propagation in realistic 3-D structure have been performed in order to understand the mechanisms of ground motion generation and further to do reliable ground motion prediction for future earthquakes have been performed. If a source model represented by sparsely distributed point sources is used as an input to such ground motion simulations, the highly concentrated sources near the earth surface can generate artificial, and large ground motion around themselves.

Therefore, it is desired to take into account rupture propagation inside each subfault. To give rupture directivity to slips on each subfault, Wald and Heaton (1994, 1996) calculated synthetic waves from many point sources over each subfault (25 point sources in Wald, 1996) and summed them up considering rupture time delays (SM). Interpolation technique was used in their work to reduce the amount of computation of the Green's functions.

In the present study, by convolving a function representing bi-directional moving-dislocation on each subfault with the point source synthetic wave from each subfault center (CM), we get an approximate synthetic wave from a uniformly distributed slip inside the subfault successively activated and propagating into arbitrary directions (Fig.1, right).

The representation of moving dislocation effect in convolutional form is first formulated by Ben-Menahem (1961). He evaluated Love wave and Rayleigh wave from a finite moving source and showed that source dimension and rupture propagation velocity play important roles in radiation pattern when the size of source becomes order of dominant wavelength of radiated waves. Aki (1968) added unidirectional moving dislocation effect to grid point sources using this method in forward modeling of the observed waveforms recorded at 80m distance from the causative fault during the 1960 Parkfield earthquake.

When a station-subfault distance is large compared with the linear dimension of the subfault, directivity effect given to waveforms by CM is close to those given by SM summing an infinite number of point sources. In CM, however, the Green's functions from a certain finite source area are approximated to be the same after phase correction and it gives large errors in the synthetics when station-subfault distance is small compared with subfault dimension. We suppress the error to a given maximum value using a relation between the error and subfault size, distance, and wavenumber obtained through a numerical test in our previous work (Sekiguchi, 1999).

The inverted rupture process using the element source waves by CM has continuous slip distribution even inside each subfault. The obtained moment release time history on a subfault directly reflects the slip time function at any point on the subfault. Such a model, used as an input of near-source ground motion simulation, avoid the problem of artificial, and large ground motions around the point sources due to the use of sparsely distributed point sources.

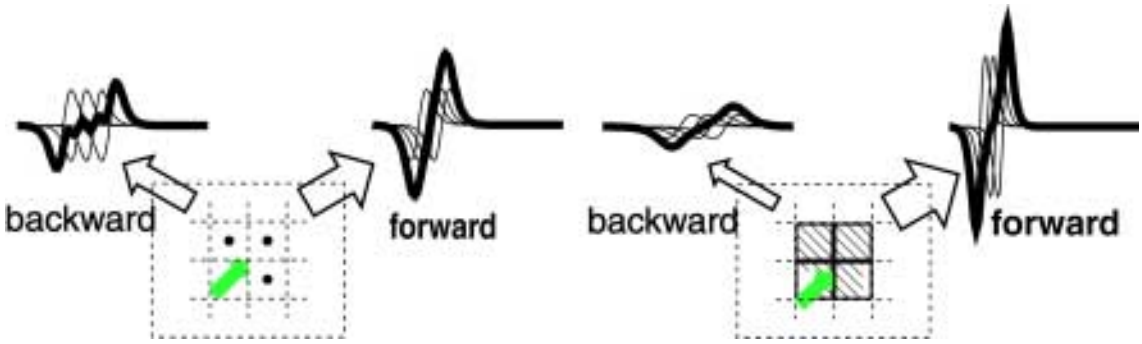

Figure 1: Schematic explanation of difference in rupture directivity effect expected to appear in the waveforms between caused by with (right) and without (left) considering rupture propagation inside each element source area.

METHOD

Moving dislocation inside subfaults by convolution in a homogeneous media

The representation of moving dislocation effect in the convolutional form in a homogeneous media is deduced as follows, being modified from Sato (1969). We consider a rectangular subfault (Σ) with length L and width W on $f\dot{I}_1 f\dot{I}_2$ -plane, dislocations parallel to the plane uniformly distributed inside the subfault, and a propagating rupture on it. A displacement field from this extended source is,

$$U_n(\mathbf{x},t) = \iint_\Sigma m_{pq}(\mathbf{f\dot{I}},\tau) * G_{np,q}(\mathbf{x},t;\mathbf{f\dot{I}},\tau) d\mathbf{f\dot{I}}$$
$$= \iint_\Sigma \sum\nolimits_{p=\xi 1,\xi 2} m_{pf\dot{I}_3}(f\dot{I}_1, f\dot{I}_2,\tau) * G_{np,f\dot{I}_3}(\mathbf{x},t;f\dot{I}_1,f\dot{I}_2\tau) df\dot{I}_1 df\dot{I}_2 \qquad (1)$$

where $m_{pq}(\mathbf{f\dot{I}},\tau)$ is the moment density tensor representing dislocation in p-direction on a plane normal to q-direction at a position $\mathbf{f\dot{I}}$, and $G_{np,q}(\mathbf{x},t;\mathbf{f\dot{I}},\tau)$ is a spatial derivative of Green's tensor representing nth component of a displacement response at a point $\mathbf{x}$ to the impulse source $m_{pq}(\mathbf{f\dot{I}},\tau)$. When the extension of the subfault is much smaller than the distance between a reference point (the center of the subfault) and a station, and 2nd (higher) order micro terms in difference of two distances; one between the reference point $((f\dot{I}_1, f\dot{I}_2) = (0,0))$ and a station and one between an arbitrary point on the subfault and the station, is negligible, the Green's function from an arbitrary point on the subfault to the station approximates to that from the reference point after correcting time delay due to difference of location (hereafter, we call it "plane wave approximation".)

$$G_{np,q}(\mathbf{x},t;f\dot{I},\tau) \cong G_{np,q}(\mathbf{x},t-t_d;\mathbf{0},\tau), \qquad t_d = \frac{1}{c}\left(\frac{f\dot{I}\mathbf{x}}{R}\right) = \frac{1}{c}\left(\frac{\xi_1 x_1 + \xi_2 x_2}{R_{\xi_1\xi_2}}\right) \qquad (2)$$

where (x_1, x_2) is a station location in the subfault coordinate, $R_{f\dot{I}_1 f\dot{I}_2}$ is distance between the reference point and the station projected onto the $f\dot{I}_1 f\dot{I}_2$ -plane $\left(R_{f\dot{I}_1 f\dot{I}_2} = \sqrt{x_1^{\,2} + x_2^{\,2}}\right)$, c is P- or S-wave velocities (V_P and V_S) at the source location. A condition to be satisfied for making the plane wave approximation is the same as what should be satisfied for the region of Fraunhofer diffraction in optics (Aki and Richards, 1980).

$$l^2 << \frac{\lambda R}{2} \qquad (3)$$

where l, λ, R are linear dimensions of a source area, wavelength, and distance between a receiver and the source. We assume a common moment release function (i.e., common mechanism and time history) over a subfault and linear rupture front propagation whose velocity in $f\dot{I}_1$ and $f\dot{I}_2$ directions are V_{r1} and V_{r2}, respectively, then,

$$m_{p\xi_3}(\xi_1,\xi_2,\tau)\Big|_{p=\xi_1,\xi_2} = m_{0\,p\xi_3}\left(0,0,\tau - \frac{\xi_1}{V_{r1}} - \frac{\xi_2}{V_{r2}}\right)\Big|_{p=\xi_1,\xi_2} \qquad (4)$$

Substituting Eq.(2) for S-wave part (direct S-wave is dominant in the waveform inversion) and Eq.(4) into Eq.(1), we get,

$$U_n(\mathbf{x},t)$$
$$= \sum_{p=\xi_1,\xi_2} \left\{ \iint_{\Sigma} m_{0\,p\xi_3} \left(0,0,\tau - \frac{\xi_1}{V_{r1}} - \frac{\xi_2}{V_{r2}} \right) * G_{np,\xi_3} \left(\mathbf{x}, t - \frac{1}{Vs} \left(\frac{\xi_1 x_1}{R_{\xi_1\xi_2}} + \frac{\xi_2 x_2}{R_{\xi_1\xi_2}} \right); 0,0,\tau \right) d\xi_1 d\xi_2 \right\} \quad (5)$$

Taking Fourier transform of both sides of the above formula,

$$U_n(\mathbf{x},\omega)$$
$$= \sum_{p=\xi 1,\xi 2} m_{0\,p\xi_3}(0,0,\omega) G_{np,\xi_3}(0,0,\omega) LW \frac{\sin Xs}{Xs} \frac{\sin Ys}{Ys} \quad (6)$$

with

$$Xs = \frac{\omega L}{2Vs} \left(\frac{Vs}{Vr_1} - \frac{x_1}{R_{\xi_1\xi_2}} \right) \qquad Ys = \frac{\omega W}{2Vs} \left(\frac{Vs}{Vr_2} - \frac{x_2}{R_{\xi_1\xi_2}} \right) \quad (7)$$

From Eq. (6) it is understood that displacement field from a rectangular finite moving dislocation is obtained by convolving Green's function with a common moment density function and a "finite moving dislocation function",

$$\frac{\sin Xs}{Xs} \frac{\sin Ys}{Ys} \quad (8)$$

We can extend the above formulas to a case of a heterogeneous media by changing t_d in (2) as,

$$t_d = \frac{1}{Vs} \left(f\grave{I}_1 r0_1 + f\grave{I}_2 r0_2 \right). \quad (9)$$

where $\mathbf{r0} = (r0_1, r0_2, r0_3)$ is a takeoff vector of ray at the source. Then Eq. (7) becomes,

$$Xs = \frac{\omega L}{2Vs} \left(\frac{Vs}{Vr_1} - r0_1 \right), \qquad Ys = \frac{\omega W}{2Vs} \left(\frac{Vs}{Vr_2} - r0_2 \right) \quad (10)$$

Practically, we perform ray tracing to obtain the takeoff vector of direct S-wave ray for each subfault-station pair.

Validity and Limitation of the Convolution Method.

As we saw in the previous section, the applicability of CM is based on the plane wave approximation assumption. However, the condition of applying this approximation, the Fraunhofer inequality (Eq. (3)), is qualitative and cannot be used to estimate the approximation error. We have made numerical tests and found that the approximation error is almost proportional to the right side of the Fraunhofer inequality condition divided by the left side (hearafter, we call it C_{fraun}) for fixed slip mechanism, rupture propagation direction and takeoff direction of the ray path (Sekiguchi, 1999). In a condition of direction, rupture propagation direction, and ray's takeoff direction to give the maximum error, it becomes 10% at distance R=16.3km. By calculating C_{fraun} value, we can judge whether only one Green's function from a reference point inside a subfault to a station is enough to approximate to a path effect between any point inside the subfault and the station. If the subfault-station distance is smaller than the critical distance for a given subfault size from the viewpoint of C_{fraun}, we can divide the subfault into smaller pieces so that the piece size satisfy the $C_{fraun} > C_{fraun,critical}$. Then we can apply CM for each piece.

APPLICATION TO THE WAVEFORM INVERSION

Flow of Preparation of Element Source Waveforms Including Rupture Propagation inside Each Subfault for the Waveform Inversion.

On introducing CM to calculation of element source waveforms for the waveform inversion, we take the following process (Fig. 3) taking into account the applicability condition examined in the previous section. After locating model fault planes and discretizing them into small subfaults, we calculate distances between every pair of subfault and station. If the distance between a pair of subfaut and station is larger than the critical distance to give a certain level of maximum error for a given subfault size, we calculate one Green's function between the center of the subfault and the station, and convolve it with the "finite moving dislocation function" and the element slip time function (Eq.(6)). If the distance is smaller than the critical subfault-station distance, we calculate the critical source size to satisfy $C_{fraun} > C_{fraun,critical}$ for the distance, subdivide the subfault into smaller pieces so that the size of the pieces is smaller than the critical source size, calculate the Green's functions between point sources on all the pieces and the station, convolve them with the "finite moving dislocation function" and the element slip time function, then sum them up considering the rupture time delays to get one element source waveform for one subfault. We can rewrite Eq. (6) when subdividing of a subfault into smaller pieces is required.

$$U_n(\mathbf{x},\omega) =$$

$$\sum_{i=1}^{Ns^2}\sum_{p=\xi_1,\xi_2}\left[m_{0\xi_3}(0,0,\omega) * G_{np,\xi_3}\left(\xi_{0_i1},\xi_{0_i2},\omega\right)\frac{LW}{N_s{}^2}\frac{\sin Xs_i}{Xs_i}\frac{\sin Ys_i}{Ys_i}\exp\left\{ i\omega\frac{\xi_{0_i1}}{V_{r1}} + i\omega\frac{\xi_{0_i2}}{V_{r2}}\right\}\right], \quad (11)$$

with

$$Xs_i = \frac{\omega L}{2V_s N_s}\left(\frac{V_s}{V_{r_1}} - r_{0_i1}\right), \qquad Ys_i = \frac{\omega W}{2V_s N_s}\left(\frac{V_s}{V_{r_2}} - r_{0_i2}\right), \quad (12)$$

where $N_s{}^2$ is the number of the subdivision required. $\left(f\grave{I}_{0_i1}, f\grave{I}_{0_i2}\right)$ is the coordinate of the center of *i*th piece and R_i is the distance between the point $\left(f\grave{I}_{0_i1}, f\grave{I}_{0_i2}\right)$ and the station projected onto the $f\grave{I}_1 f\grave{I}_2$ -plane.

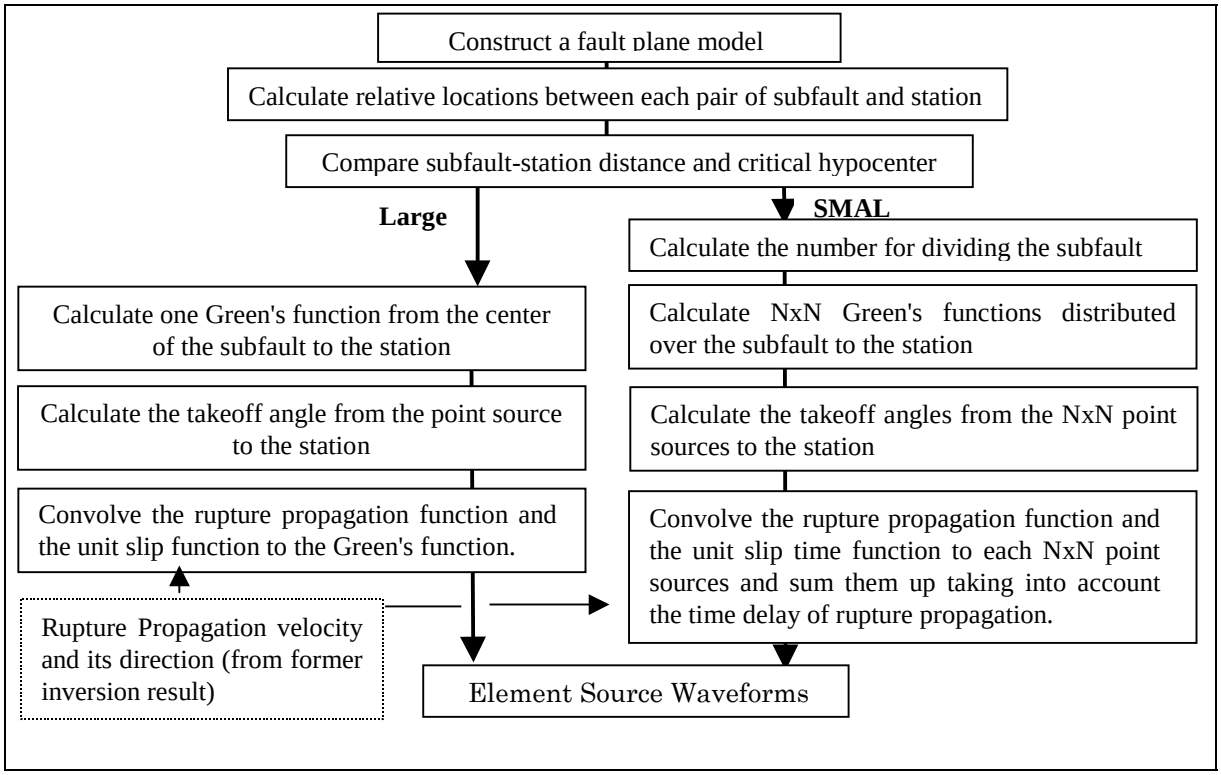

Figure 2: Flow for calculation of element waveforms with finite moving dislocation effect for the waveform inversion.

Application to the Source Inversion of the 1995 Hyogo-ken Nanbu (Kobe) Earthquake

We apply CM in the waveform inversion for the source process of the 1995 Hyogo-ken Nanbu earthquake. We use the same fault plane model and same data set (Table 1) as that in Sekiguchi et al. (1998) (Fig.3, left) taking into account the surface rupture trace of the Nojima fault, the distribution of aftershocks occurring within 18 hours after the earthquake (Nemoto et al., 1996), the static displacement determined from triangulation (Hashimoto et al. 1996), SAR (Synthetic Aparture Rader) interferograms (Murakami et al., 1995), and the particle motion rotations observed very close to the causative fault (Sekiguchi et al., 1996). The fault plane is descretized into 310 subfaults, each of them has 2.05km length and 2.05km width. For this size of subfault, the critical hypocenter distance of 10% misfit is about 13.5km. Most of station-subfault pairs have larger hypocenter distances than the critical hypocenter distance, and for such pairs only one Green's function on a subfault is enough to well approximate the responses at the station to distributed slips over the subfault. For the station-subfault pairs with smaller distances than the critical hypocenter distance, subdivision of the subfaults is required. Figure 3 (right) shows how the subfaults should be divided for calculating moving-dislocation element source waveforms at KBU station in order to hold down the plane wave approximation error within 10% in misfit. The rupture propagation velocity vectors to be convolved with each Green's function were calculated from the source model of Sekiguchi et al.(1998), assuming that the rupture arrival at each subfault is the time when the moment release exceeded 10% of the total moment release.

Table 1: Observed seismograms used in this analysis.

Station	Lat.	Lon.	Organization
AMC	34.7180	135.4080	CEORKA
CHY	34.4390	135.6590	CEORKA
KBU	34.7250	135.2400	CEORKA
MOT	34.7250	135.2810	CEORKA
TDO	34.4800	135.4080	CEORKA
TOY	34.8010	135.5010	CEORKA
AID	34.940	134.168	JMA
AIO	33.792	134.452	JMA
AWA	34.336	134.908	JMA
HEG	34.653	135.685	JMA
KOB	34.69	135.18	JMA
KOY	34.218	135.593	JMA
MRT	33.2483	134.1800	JMA
OKA	34.6583	133.9183	JMA
OSA	34.6783	135.5217	JMA
WAC	35.283	135.402	JMA
NKY	34.9667	135.6222	Kansai Electric Power Co. Inc.
SOK	34.7431	135.4417	Kansai Electric Power Co. Inc.
KMT	34.383	135.35	RRI, Kyoto Univ.
ABU	34.8600	135.5735	RCEP DPRI, Kyoto Univ.
KN1	34.855	135.217	Matsumuragumi Co. Inc.
NRT	34.234	134.641	Honshu-Shikoku Bridge Public Corporation
TZK	34.8083	135.3437	Railway Technical Research Institute
RKI	34.6883	135.2728	Sekisui House Co. Inc.
KPI	34.670	135.208	Kobe City

The multi-time window linear waveform inversion methodology (Hartzell and Heaton, 1983) is applied to estimate the source process. The moment release spatio-temporal distribution is represented by a set of element sources descretized in space and in time. As already mentioned, the model fault plane is divided into 2.05km square subfaults located at 2.05km intervals in strike and dipping directions. The moment release at any point on the model fault plane is represented by the successively activated eight smoothed ramp functions, each of which have a unit duration of 0.6 s at 0.4 s time intervals. The time windows therefore partially overlap each other. The triggering time of the first time window assigned to each subfault is calculated from the source model of Sekiguchi et al. (1998). As this inverse problem includes underdetermined model parameters, we impose two constraints; one for restricting rake angle variation range and one to smooth out moment release vectors among adjacent model parameters with a strength proportional to inverse of a distance between model parameters in spatio-temporal domain (Sekiguchi et al., 1998).

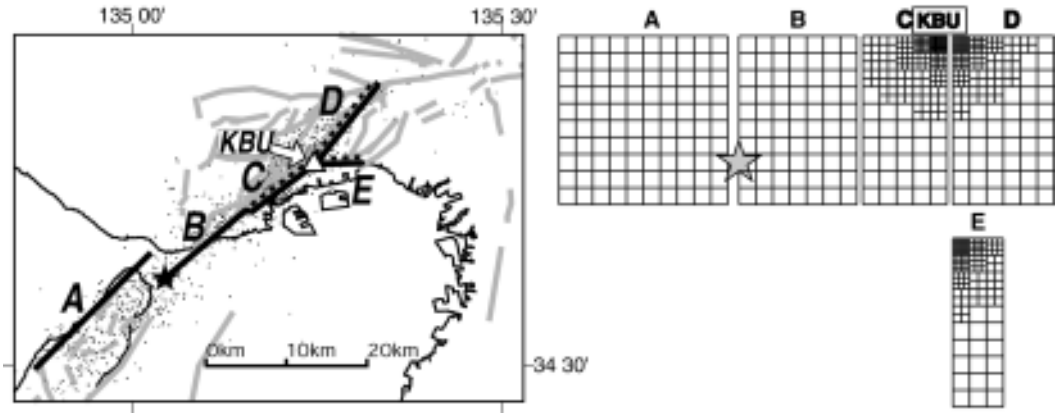

Figure 3: (Left) Fault plane model for the waveform inversion for the source process of the 1995 Hyogo-ken Nanbu earthquake. Gray lines show the active fault traces from Ishihara et al. (1991). Epicenters of the mainshock and aftershock during the day of the mainshock occurrence are determined by Nemoto et al. (1996, 1997). Circles are epicenters of aftershocks since just after till 18 hours after the mainshock. (Right) Subdivision of subfaults in order to apply CM for computation of element source waveforms at KBU station (see the map in the left) keeping the approximation error less than 10%.

INVERSION RESULTS

Figure 4, left (b) shows the time progression of moment release on the model fault plane. General features of the moment release distribution obtained using the element source waveforms without the finite moving dislocation effect (Fig. 4, left (a), after Sekiguchi et al., 1998) and with moving dislocation effect (Fig.4, left (b)) are similar each other; areas of relatively large moment release (subevents) at shallow part on the segment A, around the rupture starting point on the segment B, at deep part on the segment C, a subevent smaller than the previous three at deep part on the segment E. But the places where the peak of the moment release appears in each subevent area are different.

Figure 4, right shows the slip velocity time function obtained for each subfault. Long duration and high slip velocity at shallow part of the segment A catch our eyes. Positive correlation between final slip and peak slip velocity are observed. The relation varies for different segments. On the segment B, slip velocities tend to be larger values for certain final slip values than on the other segments.

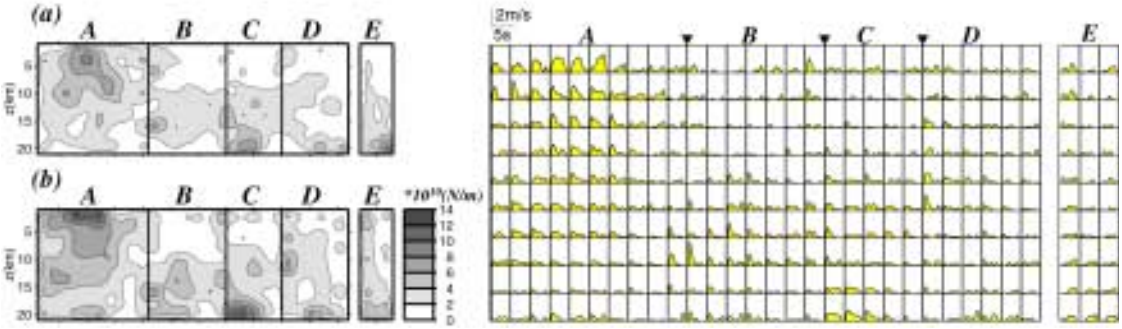

Figure 4: (Left) Total moment release density (a) using point source element waveforms (Sekiguchi et al., 1998), and (b) using element source waveforms from finite moving dislocation using CM.

(Right) The slip velocity time function on each subfault for the result shown in the left (b).

CONCLUSIONS

We introduced a convolution method (Ben-Menahem, 1961) which incorporates the effect of a moving dislocation over a finite area with a point source synthetic waveform in the calculation of element source waveforms used in the waveform inversion for earthquake rupture process. Each of such element source waves includes the effect of rupture directivity itself. Therefore, the rupture directivity effect on the entire fault area is fully considered in the waveform inversion.

The inverted rupture process by this method has a smooth slip distribution even inside the subfaults. Obtained moment release history for each subfault directly reflects a slip time function on the subfault because the rupture propagation effect inside each subfault is separated. Near-source ground motion simulation using the source

model obtained by this method escapes from the problem of artificial, and large ground motion near the point sources due to the use of sparsely distributed point sources.

We applied a convolution method (Ben-Menahem, 1961) which incorporate the effect of moving dislocation over a rectangular area to a point synthetic into computation of element source waves in the waveform inversion for the source process of the 1995 Hyogo-ken Nanbu earthquake. The overall characteristics of the moment release distributions are similar between two inversion results; one inverted with point source element waveforms and the other with element source waves considering the finite moving dislocation effects inside each subfault. But details like places of peak moment releases differ between these inversion results. Positive correlation between final slip and peak slip velocity are observed.

ACKNOWLEDGMENTS

We thank the organizations who provided us with recordings; the Committee of Earthquake Observation and Research in the Kansai Area; Japan Meteorological Agency; Kansai Electric Power Co. Inc.; the Port and Harbor Research Institute; the Research Center of Earthquake Prediction of the Disaster Prevention Research Institute, Kyoto University; the Research Reactor Institute, Kyoto Univ.; the Public Works Research Institute (1995); Kobe City, Sekisui House Co. Inc.; Matsumuragumi Co. Inc.; and Railway Technical Research Institute (Nakamura et al., 1996) (serial no. 032). We thank Takao Kagawa for providing us the restored recordings at KBU and MOT stations. We thank Olivier Coutant who originally coded the program to calculate Green's function for layered media. We thank Andreas Rietbrock for advises. We used GMT (Genetic Mapping Tools, Ver.3.0, Wessel and Smith, 1991) for making figures.

REFERENCES

Aki, K. (1968), "Seismic Displacements near a Fault", *J. Geophys. Res*., 73, 16, pp5359-5376.

Aki, K. and Richards, P. G. (1980), *Quantitative Seismology*, W. H. Freeman and Co., San Francisco.

Ben-Menahem, A. (1961), "Radiation of seismic surface-waves from finite moving sources", *Bull. Seism. Soc. Am.*, 51, 3, pp401-435.

Hartzell, S. H. and Heaton, T. H. (1983), "Inversion of strong ground motion and teleseismic waveform data for the fault rupture history of the 1979 Imperial Valley, California, earthquake", *Bull. Seism. Soc. Am.*, 73, pp1553-1583.

Hashimoto, M., Sagiya, T., Tsuji, H., Hatanaka, Y. and Tada, T. (1996), "Coseismic displacements of the 1995 Kobe earthquake", *J. Phys. Earth*, 44, pp255-279.

Ishihara, M., Yoshikawa, S., Mitamura, M., Mizuno, K. and Hayashi, T. (1991), "1:125,000 Quaternary Geological Map of Osaka and Adjacent Areas, Kinki, Japan", *Urban Kubota*, 30, (in Japanese).

Murakami, M., Fujiwara, S. and Saito, T. (1995), "Detection of Crustal Deformations associated with 1995 Hyogoken-Nanbu earthquake by interferometric SAR", *Current News of Geophysical Survey Institute of Japan*, 83, pp24-27.

Kagawa, T., Irikura, K. and Yokoi, I. (1996), "Restoring clipped records of the near field strong ground motion during the 1995 Hyogo-ken Nanbu (Kobe), Japan, earthquake", *J. Natural Disas. Sci.*, 18, 1, pp43-57.

Nakamura, Y., Uehan, F. and Inoue, H. (1996), "Waveform and its analysis of the 1995 Hyogo-ken Nanbu earthquake (II)", *JR Earthquake Information No. 23d*, Railway Technical Research Institute, (in Japanese).

Nemoto, H., Katao, H., Suzuki, E., Yoshida, Y. and Irikura, K. (1996), "The spreading of aftershocks area directly after the 1995 Hyogo-ken Nanbu earthquake", *Programme and Abstracts Seism. Soc. Japan 1996 No.2*, (in Japanese).

Sato, R. (1969), "Formulations of solutions for earthquake source models and some related problems", *J. Phys. Earth*, 17, 2, pp101-110.

Sekiguchi, H., Irikura, K., Iwata, T., Kakehi, Y. and Hoshiba, M. (1996), "Minute locating of faulting beneath Kobe and the waveform inversion of the source process during the 1995 Hyogo-ken Nanbu, Japan, earthquake using strong ground motion records", *J. Phys. Earth*, 44, pp473-487.

Sekiguchi, H., Irikura, K. and Iwata, T. (1999), "Fault Geometry in the Rupture Termination of the 1995 Hyogo-ken Nanbu Earthquake", submitted to *Bull. Seism. Soc. Am*.

Sekiguchi, H. (1999), "Rupture process analysis of the 1995 Hyogo-ken Nanbu earthquake, a doctoral thesis presented to the graduate school of science", Kyoto University.

Somerville, P., Smith, N. F., Graves, R. W. and Abrahamson, N. A. (1997), "Modification of empirical strong ground motion attenuation relations to include the amplitude and duration effects of rupture directivity", *Seism. Res. Lett*., 68, pp199-222.

Wald, D. J. (1996), "Slip history of the 1995 Kobe, Japan, earthquake determined from strong motion, teleseismic, and geodetic data", *J. Phys. Earth*, 44, pp489-503.

Wessel, P. and Smith, W. H. F. (1991), "Free software helps map and display data", *EOS Trans Amer. Geophys. U.*, 72, 441, pp445-446.